Geotechnical Testing Journal

doi:10.1520/GTJ20180352 / Vol. 43 / No. 4 / 2020 / available online at www.astm.org

Carlos Rodrigues,[1] Nuno Cruz,[2,3] Sara Amoroso,[4,5] and Manuel Cruz[6]

Stiffness Decay in Structured Soils by Seismic Dilatometer

Manuscript received May 15, 2018; accepted for publication July 19, 2019; published online September 6, 2019. Issue published July 1, 2020.

[1] Civil Engineering Department, Polytechnic Institute of Guarda, Avenida Dr. Francisco Sá Carneiro 50, Guarda, Guarda 6300-559, Portugal, https://orcid.org/0000-0003-1054-0468

[2] Geotechnical Department, MOTA-ENGIL, S.A., Rua Rêgo do Lameiro 38, Porto, Porto 4300-454, Portugal (Corresponding author), e-mail: nunocruz@mota-engil.pt, https://orcid.org/0000-0002-1247-6108

[3] Department of Geosciences of University of Aveiro, Campus Universitário de Santiago, Aveiro 3810-193, Portugal

[4] Istituto Nazionale di Geofisica e Vulcanologia, L'Aquila, Viale Crispi 43, 67100, Italy, https://orcid.org/0000-0001-5835-079X

[5] Department of Engineering and Geology, University of Chieti-Pescara, Viale Pindaro 42, Pescara 65129, Italy

[6] Mathematical Engineering Lab, Polytechnic Institute of Porto, Rua Dr. António Bernardino de Almeida 431 Porto, Porto 4200-072, Portugal

Reference

C. Rodrigues, N. Cruz, S. Amoroso, and M. Cruz, "Stiffness Decay in Structured Soils by Seismic Dilatometer," *Geotechnical Testing Journal* 43, no. 4 (July/August 2020): 1003–1021. https://doi.org/10.1520/GTJ20180352

ABSTRACT

The small-strain stiffness modulus G_0 is not directly applicable to evaluate deformation in most practical engineering problems, and therefore, nonlinear soil behavior curves have been developed in terms of Young modulus E or shear modulus G. These curves were successfully obtained for sedimentary soils, while for residual soils, the available data from intertional community is still scarce. Residual soils are considered structured soils and often classified as problematic soils since they do not fit into the behavior of remolded or unstructured soils. In fact, the role of bonding and fabric affects both the strength and the stiffness of the soil. This article illustrates the use of the seismic dilatometer test (SDMT) for the determination of in situ stiffness decay curves with strain level (G-γ curves or similar) in a granitic residual soil of the Northeastern region of Portugal (Guarda), showing its adequacy to solve these kinds of problems. In situ and laboratory tests were performed on these granitic residual soils. The adopted approach relies on the ability of SDMT to provide a small-strain modulus G_0 (from the shear wave velocity V_s) and a "working strain" modulus G_{DMT} (derived from the constrained modulus M_{DMT} in accordance with the theory of elasticity). Thus, in situ G-γ decay curves were tentatively constructed by fitting curves through these two points using a hyperbolic model. However, it was observed that the results obtained by the hyperbolic model for the cemented soils are not satisfactory. Based on the SDMT parameters, a logistic curve was derived for the reproduction of reference stiffness curves obtained from the triaxial test results.

Keywords

stiffness decay curves, structured soils, nonlinear soil behavior, seismic dilatometer test

Introduction

Small-strain shear modulus is actually considered one of the most important parameters to describe stiffness behavior for design purposes. The nonlinear behavior of soils with no

apparent microstructure has been deeply studied through stiffness decay curves with strain level, showing that the decay is variable with the soil nature and, in particular, is more pronounced for sands rather than for silts and clays. On the contrary, in the case of residual soils evolving from weathering processes of rocks, the established methodologies seem to produce important deviations from reality. The soils resulting from weathering of granites are commonly studied for this purpose (e.g., Rocchi and Coop 2015; Viana da Fonseca and Coutinho n.d.), with their structure depending on two fundamental parts: the interparticular bonds that continuously change with the weathering progress and the fabric of the soil inherited from the intact rock. The evolution of loading on these soils is followed by a decrease of stiffness, which is characterized by the occurrence of characteristic points, known as yield points, which are related to specific states of the soil. As such, the initial breaking of the weak bonds corresponds to the first yield, where the evolution toward this point is identified by a plateau of the stiffness that corresponds to the elastic behavior. With the load increase, more bonds will break, reaching a point at which the soil structure cannot tolerate any additional load without collapsing. At this point a sharp decrease in soil stiffness can be detected, and it is designated as bond yield (Malandraki and Toll 2001) or gross yield (Coop and Willson 2003; Alvarado, Coop, and Willson 2012). From this point on, the residual soil behaves like a destructured one, converging with the principles of classical soil mechanics.

From the deformability point of view, in the strain range in which soils (sedimentary or residual) exhibit a real elastic behavior, i.e., in which they recover almost completely, the applied strain is very small and the soil stiffness decays nonlinearly with the increase of the strain level, following a well-known S-shaped reduction curve using a semilogarithmic graph. Several authors used this representation to study the stiffness decay behavior of structured soils (Cuccovillo and Coop 1997; Clayton and Heymann 2001; Coop and Willson 2003), while other authors preferred to use the bilogarithmic representation (Malandraki and Toll 1996).

The seismic dilatometer test (SDMT) has been increasingly used to evaluate these nonlinear properties because of its ability to provide a small-strain shear modulus G_0 from the shear wave velocity V_s and a working strain shear modulus at a medium strain level G_{DMT}. This modulus is derived from the constrained modulus M_{DMT} (or M) in accordance with the theory of elasticity, as stated by Marchetti et al. (2008) and Amoroso et al. (2014). Moreover, Monaco et al. (n.d.) argued that since M_{DMT} is a working strain modulus, the ratio G_{DMT}/G_0 could be regarded as the shear modulus decay factor at working strains since G_{DMT} is obtained through the theory of elasticity from M_{DMT}. This approach was followed with success by Di Mariano et al. (2019), estimating the stiffness dependence on the stress-strain level by the finite-element model of a deep excavation.

Furthermore, the Marchetti dilatometer test (DMT) equipment possesses some important characteristics for these determinations, starting from the fact that test measurements include pressure measurements related to specific displacements obtained in a phase separated from the penetration, which is not so common in other penetration devices. On one hand, during the penetration phase, the very low apical angle and flat shape of the blade generate a low level of damage to the soil structure (Baligh and Scott 1975; Huang 1989; Whittle and Aubeny n.d.; Finno 1993). The membrane location is in the optimal zone for low-to-medium strain level (Whittle and Aubeny n.d.; Ishihara n.d.; Mayne n.d.), and its dimension ensures a significant volume of soil involved in the measurement phase. In fact, the 60-mm diameter creates a stress bulb at least equal to the diameter of the membrane, reducing the effect of damage on the soil structure involved in the measurements. Globally, the penetration of the blade partially affects the cementation structure, positioning the DMT measurement between first yield and bond (gross) yield, with lower strain as the cementation magnitude increases (Cruz 2010). Since first yield represents the beginning of the cementation breakage that only finishes in the bond yield, then the DMT measurements are obtained under the influence of cementation. Finally, anisotropy effects are not expected in these granitic residual soils.

The study based on SDMTs and triaxial tests (TRXs) presented herein aims toward the development of models representing in situ stiffness decay curves, applicable to structured soils. The experimental work was performed in granitic residual soils of the Northeastern region of Portugal (Guarda) included in a vast geotechnical data set of Porto and Guarda residual massifs used in several research frames of DMT in residual soils, as summarized in Cruz (2010).

Site Characterization

The framework discussed in this article is based in the Polytechnic Institute of Guarda (IPG) experimental site facilities. This study is part of a larger research work developed to contribute to the knowledge of the Portuguese granitic residual soils behavior and promote the development of specific methodologies to derive strength and stiffness parameters from in situ test results, with special emphasis on (S)DMT and (seismic) piezocone tests ((S)CPTus; e.g., Rodrigues 2003; Cruz 2010). This aspect has particular relevance since the available correlations found for sedimentary soils are generally not applicable in structured soils.

The research work at the IPG site started at the end of the nineties with a full laboratory and in situ characterization of the local residual soil deposit (Rodrigues 2003). Departing from this earlier characterization, a special testing program based on artificially cemented soils was established by Cruz (2010), aiming to correlate the results of a DMT test with soil strength and stiffness parameters. This experiment was carried out in a large-scale controlled-condition chamber (CCC). A vast amount of data from the Porto Geotechnical Map (COBA 2003) were used in the global study.

The successful work with the referred DMT calibration opened the door to implement identical frameworks dedicated to CPTus and Menard pressuremeter tests (PMTs). Therefore, a new testing program was carried out, consisting of six sets of SDMTs, SCPTus, and PMTs as well as boreholes and sampling for TRXs (Phase 3; **fig. 1**). The SDMTs allowed for regularly measuring shear wave velocities with depth, which were scarcely available in the previous investigation phases. **Table 1** shows a summary of the tests performed in each stage of the research. Detailed information on the previous works can be found in Rodrigues (2003) and Cruz (2010).

GEOLOGICAL BACKGROUND

The city of Guarda is located in a granitic mass designated as the Guarda Granitic Formation, and it is part of the geological complex related to the formation of "Serra da Estrela," the highest mountain in the Portuguese

FIG. 1 Spatial localization of the in situ tests of Phase 3.

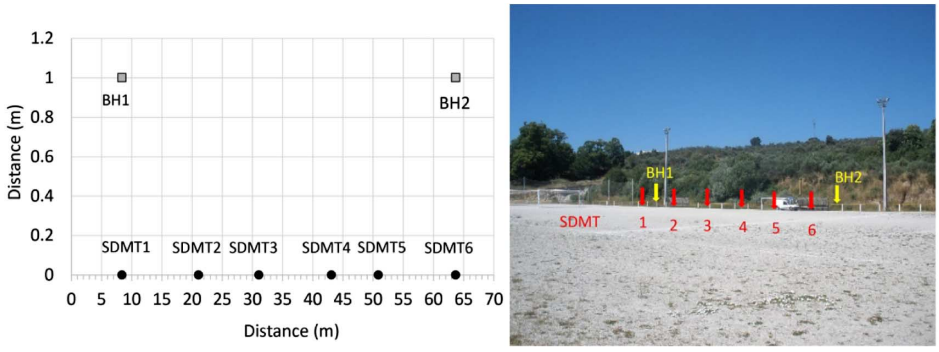

TABLE 1
Tests performed in IPG experimental site

Phase	Target	Tests	Reference
1	Characterization of residual mass (natural samples)	PMT (5), CPTu (3), DMT (2), triaxial (5), UCS (12), CH (1)	Rodrigues (2003)
2	DMT calibration (artificial cemented mixtures)	SDMT on large-scale specimens (5), triaxial (5), UCS (30), diametral compression (30)	Cruz (2010)
3	CPTu, PMT calibration (natural samples)	SDMT (6), PMT (18), SCPTu (6), triaxial (6)	–

Note: PMT = Menard pressuremeter test; (S)DMT = (seismic) Marchetti dilatometer test; CH = cross-hole test.

mainland. From the lithological point of view, the Guarda formation corresponds to a leucomesocratic granite composed of quartz, sodic and potassium feldspars commonly found in mega crystals, biotite, and muscovite as well as kaolin, sericite, and chlorite as main secondary minerals (Rodrigues 2003). In the Guarda region, similarly to what happens in other Portuguese regions, the wet-moderate climate favors the weathering, turning the granitic rock mass into a residual mass. The fluctuations of water level, which in the IPG site vary from a submerged stage in the wet season to depths of 2–5 m during the summer, create the conditions that facilitate the constant weathering of the rock substrate. As the weathering progresses, the primary interparticular bonds between the grains are broken, and a series of intergranular voids are created. Afterward, the weathering makes the feldspars and micas unstable, allowing the leaching to occur, thus creating a network of intragranular voids. In addition, the stable quartz grains are bonded by highly weathered (and therefore unstable) grains of feldspars and micas to form a solid skeleton that sometimes can be quite open. Typically, the Guarda residual mass is characterized by a silty sand/sandy silt with coefficients of permeability ranging from 10^{-6} to 10^{-7} m/s. The petrographic index, X_d, which relates percentages of weathered and unweathered grains as defined by Lumb (1962), falls between 0.27 and 0.64, reflecting the high weathering degrees of the local massif (Rodrigues 2003). **Figure 2** shows some characteristics of the soil deposit used in the study. The geotechnical in situ behavior of Guarda and Porto granitic residual soils is essentially the same.

GEOTECHNICAL CHARACTERIZATION

A summary of the results obtained in the whole set of the performed tests within this experimental site is presented in **Tables 2** and **3**. The results of all tests showed that the local residual mass is characterized by 2 layers of different strength and stiffness, represented by N_{SPT} values of 10–30 and 30–60, located from 1 to 5 and 5 to 9-m depth, respectively. The values are ordered in the table according to this differentiation. These two geotechnical horizons are the most frequent in the Portuguese granitic residual soils, particularly in Porto and Guarda (Cruz 2010).

FIG. 2 Soil characteristics of the massif under study. S = degree of saturation; γ = unit weight; e = void ratio; N_{SPT} = penetration resistance.

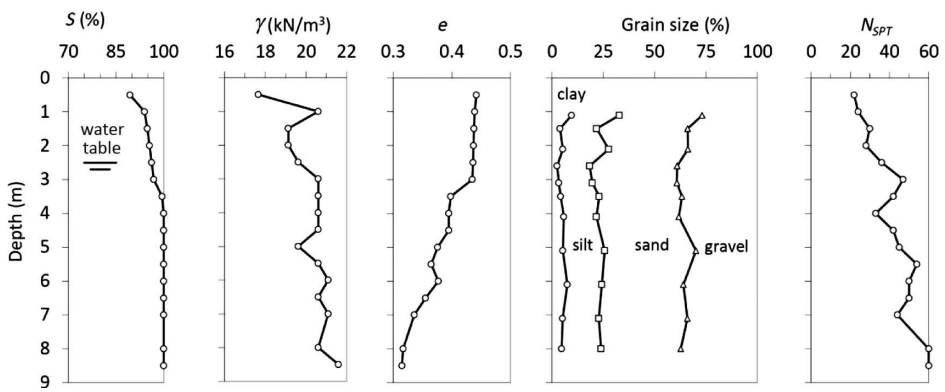

TABLE 2
CPTu and PMT parameters

Depth, m	N_{SPT}	q_t, MPa	f_s, kPa	Q_{tn}	F_R, %	B_q	P_0, MPa	P_Y, MPa	P_L, MPa	E_{PMT}, MPa
1–5	10–30	5–15	100–250	250–500	1.5–2.2	0.0–0.05	0.07–0.1	0.9–1.2	1.3–1.8	10–20
5–9	30–60	15–25	250–500	300–500	1.5–3.0	−0.1–0.0	0.15–0.25	1.2–3.0	2.0–3.5	15–40

Note: N_{SPT} = blow count representation of the penetration resistance of the soil; q_t = corrected cone resistance; f_s = sleeve friction; Q_{tn} = normalized cone resistance; F_R = friction ratio; B_q = normalized pore pressure ratio; P_0 = PMT in situ horizontal stress; P_Y = PMT yield pressure, P_L = PMT limit pressure; E_{PMT} = pressuremeter modulus.

TABLE 3
Basic and intermediate DMT parameters

Depth, m	N_{SPT}	p_0, MPa	p_1, MPa	I_D	K_D	E_D, MPa
1–5	10–30	0.3–1.0	1.0–2.5	1–3	15–25	25–75
5–9	30–60	1.0–2.5	2.0–4.0	1–3.5	10–40	60–120

Note: p_0 = DMT corrected first reading; p_1 = DMT corrected second reading; I_D = material index; K_D = horizontal stress index; E_D = dilatometer modulus.

To analyze the evolution of decay curves discussed herein, triaxial, DMT, and seismic tests were taken from Phases 2 and 3 of the IPG research programs. These tests were performed in artificially cemented mixtures and also in natural structured materials within the same strength levels. The artificial samples were used because it was firstly intended to avoid both the in situ typical variability of these soils and the existing gap between in situ and laboratorial tests (caused by sampling), which can have an important impact on the cementation structure. A set of natural samples recoiled in boreholes performed side by side with SDMT tests was also included to serve as a bridge between laboratorial and natural conditions.

Tests Performed in Artificially Cemented Soils

The research frame related to DMT calibration (Phase 2) was developed in a CCC, in which the testing conditions of DMT tests could be controlled. The experiment consisted of making artificially cemented samples for the chamber and TRXs remolded in exactly the same conditions to reach comparable situations. The mixtures consisted of previously destructured residual soil (obtained in the IPG experimental site residual mass), followed by artificial cementations with different contents of portland cement. SDMT tests were previously carried out in that mass for later comparisons between CCC specimens and in situ results.

SAMPLE PREPARATION

The CCC specimens were obtained by compaction of the artificial mixture, prepared in layers 70–80 mm thick to obtain void ratios of the same order of magnitude of those observed in situ. At the end of the process, the total height of the compacted soil corresponded to 1.25 m, and 17 layers constituted it. During the compaction, two DMT blades were installed, one 20 cm above the base level and another placed 25 cm below the surface in the upper level of the CCC specimen. To control the water level, two open-tube poly(vinyl chloride) piezometers were installed, one located in one corner from which the water was introduced at the base of the chamber, and the second located in the opposite corner to confirm the water arrival and the respective level stabilization. Above water level, suction measurements were obtained by means of six installed tensiometers. Finally, three pairs of geophones for seismic survey were placed along one profile to measure compression and shear wave velocities. **Figure 3** illustrates the CCC specimen, while **figure 4** represents the location of the measurement devices. Detailed information can be found in Cruz (2010).

Specimens were prepared aiming to observe the influence of cementation level on the mechanical behavior, reproducing the in situ conditions. Of course, reproducing the fabric and cementation level simultaneously is extremely complex to achieve; therefore, specimens were formed always considering the same void ratio and varying cementation levels. In conformity, three specimens were prepared: one remolded with no added cement (Rem 0) and two mixtures with different percentages of portland cement (Mix 1 and 2). Sample Rem 0 was composed of dry destructured granitic residual soil and 10.5 % water. Mix 1 was prepared with the same dry soil, which was mixed with 1 % cement (CEM I 52,5R) and 10.5 % water. Mix 2 was composed of the dry soil but with 2 % cement (CEM II/B-L 32,5N) and 10.5 % water. Compaction tests were used to determine the characteristic values (optimum water content and maximum dry density) that allow the same void ratio observed in situ. **Table 4** presents some characteristics of the used cements. For each level of cementation, uniaxial compressive strength (UCS), diametral compression, and TRXs were performed on artificial samples remolded and cured exactly in the same conditions of those observed in CCC specimens.

The mixtures were then left in the curing process, and at predesignated days, water was introduced within the chamber until reaching 118 cm in depth, above the position of the lower blade. Regular measurements of suction

FIG. 3

(*A*) Installation device of DMT blades; (*B*) installation of seismic devices; (*C*) final aspect of a CCC specimen.

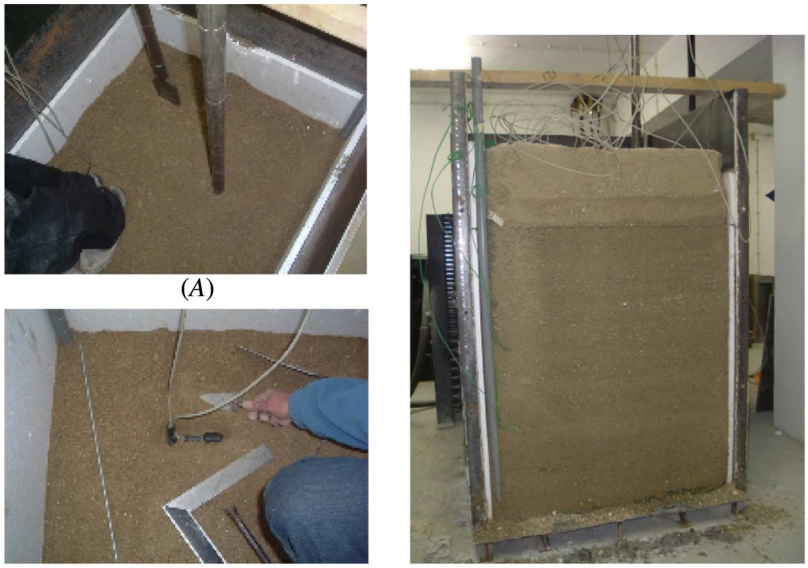

FIG. 4

Plant and cross section of the CCC instrumentation.

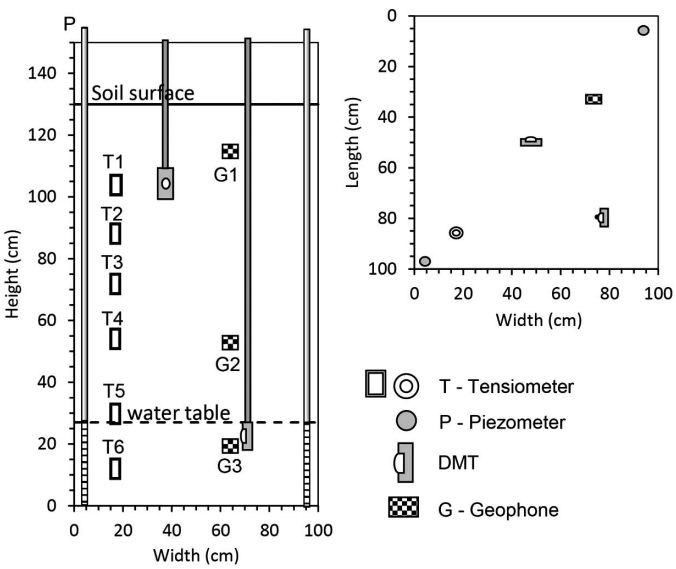

and seismic wave velocities were acquired during the curing period before and after saturation. After complete stabilization of the water level, DMT readings were taken on the first and second preinstalled blades, followed by the readings taken on the second blade pushed at regular intervals of 20 cm toward the first blade testing depth. The DMT results used in the present research were those obtained in the upper blades after they were statically pushed down to have a situation comparable with the usual test procedures, from which the curves have to be obtained. The preinstalled blade–derived results were used to study and model the penetration influence, a subject that is too complex to be discussed herein.

TABLE 4
Characteristics of the used cements

Parameter	Mix 1	Mix 2
Name	CEM I 52,5R	CEM II/B-L 32,5N
Strength class	52.5 R	32.5
Compressive strength, MPa	30.0 (2 days)	16.0 (2 days)
	52.5 (28 days)	32.5 (28 days)
Clinker	>95 %	65–79 %
Setting time, min	Start >45	Start >75
Expansion, mm	<10	<10

DMT RESULTS AND SEISMIC MEASUREMENTS

As indicated in the previous section, three sets of geophones (vertical and horizontal) were located at three different depth locations (0.2, 0.6, and 1.2 m) within the soil-cement mixtures in a vertical alignment. At each test depth, two geophones were installed, one in a horizontal position and one vertical for P-wave and S-wave velocity measurement, respectively. A block of 117.6N and an impact plate lying under rolling bars composed the source for the generation of S-waves. The load was applied on the impact plate with a good coupling between the beam and the soil, improving the quality of wave propagation. The blow generates a vibratory action with higher acceleration than the one that would have been obtained considering a fixed total mass of plate and load. This configuration creates sharper signals and higher efficiency in first arrival determination (Almeida et al. n.d.). Compression and shear wave velocities were obtained after the blade installation and before and after saturation as well as during testing time.

Figure 5 shows the material index, I_D, constrained modulus, M (or M_{DMT}), and horizontal stress index, K_D, profiles obtained by DMT blades after penetration processes. DMT readings at 1.2-m depth are influenced by its position near the chamber base and thus should be neglected. On its turn, the shear modulus at small strains, G_0, was obtained by the seismic measurements using equation (1), and they are not affected by the low position of geophones because the velocity was calculated between that point and the surface, where the seismic waves were generated.

$$G_0 = \rho V_s^2 \tag{1}$$

where:

ρ = density ($\rho = \gamma/g$; γ = unit weight, g = gravity), and
V_s = shear wave velocity.

FIG. 5 SDMT test results in artificially cemented soils (pushed blades).

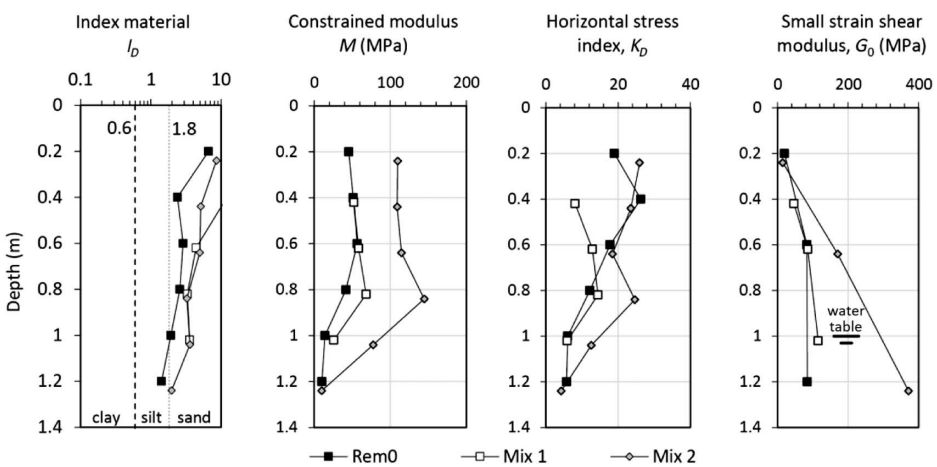

TABLE 5
Laboratorial test results in artificially cemented soils

Test	Parameter	Rem 0	Mix 1	Mix 2
UCS	q_u, kPa	20.8	72.9	124.9
Diametral compression	q_t, kPa	1.5	7.2	15.3
CID TRXs	$q_{max} = \sigma'_1 - \sigma'_3$, kPa	130	231	314

The results shown in figure 5 indicate that the evolution of the cementation level is well represented by the translation to the right (increasing cementation magnitude) of the M, K_D, and G_0 profiles related to Mix 1 and 2, although the observed difference between the mixture Mix 1 and the noncemented specimen (Rem 0) is not so clear and sometimes has random variation. In the case of K_D, the first three results of the Rem 0 profile seem abnormal when compared with the Mix 1 and 2 profiles. Apart from that, the smoother difference between the Rem 0 and Mix 1 related results can be explained by the development of suction that will hide the cementation influence when the magnitude is small. This seems to be supported by considering the tensile strength (q_t), usually considered as an index parameter for the level of cementation, that shows values of 1.5, 7.2, and 15.3 kPa, for Rem 0, Mix 1, and Mix 2, respectively (Cruz 2010). The low value of Mix 1 tensile strength and the small difference to Rem 0 can justify the apparent overlap of these two profiles. Finally, I_D profiles show convergent values for Mix 1 and 2, which in turn are higher than the Rem 0 profile. This is consistent with the known effect of cementation in the grain size distribution that shows a translation of the curve to higher diameters as a consequence of particle cementation.

TRX RESULTS

In the sequence of the preparation of the CCC specimens, identical mixtures were remolded under the same conditions (same destructured soil specimen, percentage of cement, void ratios, and curing times) to be used in TRX. The preparation consisted of 4 layers 3.5-cm thick, statically compacted using a split mold for adequate extrusion. The specimens were then stored in a curing chamber with automatic control of environmental conditions (temperature ≈ 20°C ± 1°C and humidity ≈ 95 ± 5 %). The cementation level was referenced by UCS and diametral compressive strengths instead of the percentage of cement, as these parameters are representative of the mechanical behavior and are highly influenced by the presence of cemented structures (Cruz 2010). Table 5 summarizes the results of UCS (q_u), tensile strength (q_t), and maximum deviatoric stress (q_{max}) for the confining pressure of 50 kPa obtained in TRXs.

The TRXs were performed with local instrumentation (linear variable differential transformers), namely a pair of axial transducers and a Bishop ring, for the measurement of radial deformation. The specimens were consolidated at three different stresses (50, 150, and 300 kPa) to perform isotropically consolidated drained (CID) TRXs. The stress path selected in the TRXs is similar to the stress path followed in the DMT test, corresponding to the constant σ'_3, or at a constant ratio of $\Delta q/\Delta p' = 3$ in space of stresses q and p. In this case, $q = (\sigma_1 - \sigma_3)$, $p' = [1/3(\sigma'_1 + 2\sigma'_3)]$, $\sigma'_1 = \sigma'_v$, and $\sigma'_3 = \sigma'_h$, with σ'_1 and σ'_3 representing the minimum and major principal effective stresses, respectively, while σ'_v represents the vertical effective stress and σ'_h the horizontal effective stress. The same methodology was followed with the tests performed on natural cemented soils.

Tests Performed in Naturally Cemented Soils

SDMT TESTS

The SDMT used in the experimental work is the combination of the mechanical DMT introduced by Marchetti (1980) with a seismic module for measuring the shear wave velocity, V_s (Marchetti et al. 2008), standardized in ASTM D6635-15, *Standard Test Method for Performing the Flat Plate Dilatometer*. The SDMT system incorporates a cylindrical seismic module with 2 receivers spaced 0.50 m apart above the DMT blade, working as a downhole survey according to ASTM D7400/D7400M-19, *Standard Test Methods for Downhole Seismic Testing*.

FIG. 6 SDMT test results in natural soils.

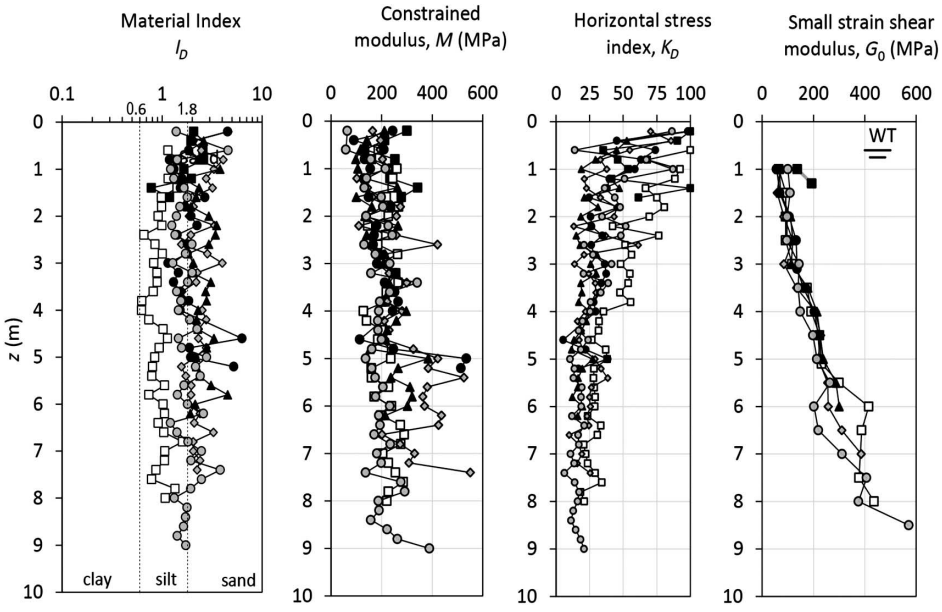

The SDMT test results obtained at the Guarda site are summarized in figure 6. From the soil identification point of view, the material index I_D is fully consistent with the grain size of these granitic residual soils, showing the adequacy of the parameter to identify these soils (Cruz 2010). The horizontal stress index K_D ranges mostly between 10 and 40, clearly pointing out a significant cementation structure in the soil, which is confirmed by the particularly high values of M_{DMT} around 200 MPa in the upper 4-m depth and 325 MPa in the lower part of the profile. These different magnitudes of the modulus clearly correspond to different weathering levels that were identified in all other performed tests. Finally, the G_0 profile shows a linear increase with the depth.

The unit weight required for determination of K_D (and, subsequently, also for M_{DMT}) was evaluated using the proposal of Marchetti and Crapps (1981). To verify its adequacy in this residual mass, DMT results were compared with the direct measurements of the unit weight obtained from the triaxial specimens collected at different depths in correspondence with two different SDMT locations (BH1-SDMT1 and BH2-SDMT6). An identical procedure was followed in the case of artificial soils. The results validate the adopted approach with the results presented in figure 7.

TRXs

A set of three undisturbed samples was retrieved with a thin sampler specifically built for these soils (Rodrigues 2003) from BH1 and BH2 boreholes 1 m distant from SDMT1 and SDMT6, respectively. Specimens of these samples were prepared and subjected to TRXs. Table 6 shows the maximum values of the deviatoric stress q_{max} and the corresponding axial strain ε_a obtained from the CID TRXs carried out at the confining pressure $p'_0 = 50$ kPa, while figure 8 shows the secant stiffness-strain behavior, obtained from the 3 samples collected at different depths and consolidated at 50 kPa. The initial value of *Gsec* for the sample BH2-3.4m (fig. 8*C*) is much lower than for the samples BH1-1m (fig. 8*A*) and BH2-1m (fig. 8*B*), which is certainly due to a higher level of disturbance of the sample taken at 3.4-m depth.

In Situ G-γ Decay Curves

The approach to establish G-γ decay curves from SDMT relies on the ability of the test to provide routinely at each depth both a small-strain modulus (G_0 from V_s) and a "working strain" modulus (G_{DMT} derived from M_{DMT}). These

FIG. 7 Comparison of values of unit weight obtained from the SDMT and triaxial specimens in (*A*) BH1 and SDMT1, (*B*) BH2 and SDMT6, (*C*) CCC and DMT in Rem 0, (*D*) CCC and DMT in Mix 1, and (*E*) CCC and DMT in Mix 2.

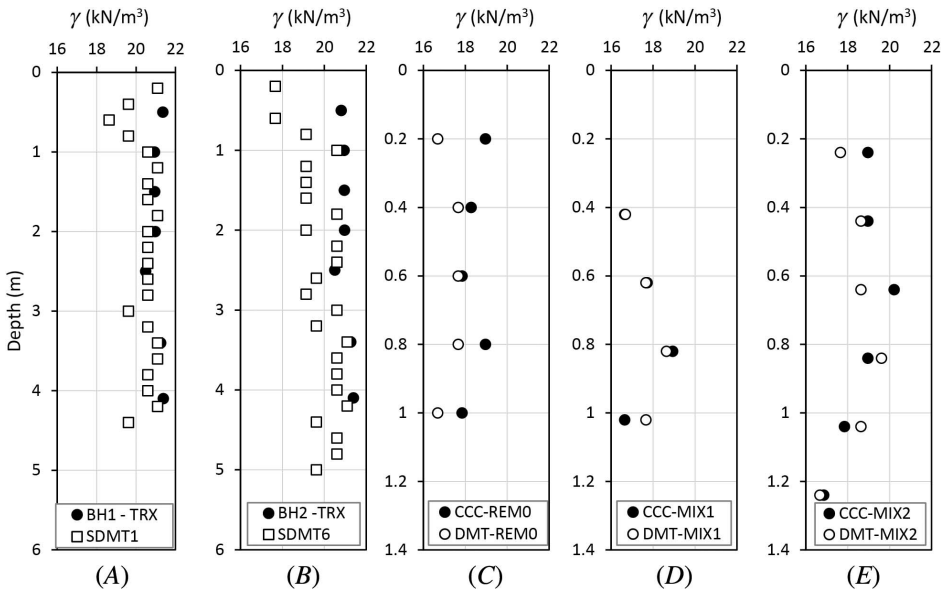

TABLE 6
Maximum deviatoric values (q_{max}) of CID TRXs ($p'_0 = 50$ kPa) in artificially cemented soils

Parameter	BH1-TRX-Depth 1.0 m	BH2-TRX-Depth 1.0 m	BH2-TRX-Depth 3.4 m
$q_{max} = \sigma_1 - \sigma_3$, kPa	273	178	287
ε_a, %	4.65	2.11	5.47

parameters could be tentatively used to develop an in situ decay curve. In the present case, G_0 was evaluated by using V_S obtained at the same depth of retrieved triaxial specimens, while G_{DMT} was derived from M_{DMT} by using the linear elastic formula (equation (2)), as suggested by Monaco, Totani, and Calabrese (n.d.) and Marchetti et al. (2008):

$$G_{DMT} = \frac{M_{DMT}}{2(1-\nu)/(1-2\nu)} \tag{2}$$

where the Poisson's ratio, ν, was assumed equal to 0.30 based on the local experience.

However, to use G_{DMT}, it is necessary to know the corresponding elemental shear strain, here designated as γ_{DMT}. In this context and for sedimentary soils, Mayne (n.d.) pointed out a range for γ_{DMT} within 0.05–0.1 %, while Ishihara (n.d.) suggests that the range can be much larger, varying from 0.01 to 1 %. Monaco et al. (2014) reconstructed soil stiffness decay curves for the Treporti case history from local vertical strains measured at the center of the embankment under each load increment, indicating that γ_{DMT} was within the range 0.02–0.14 % in sand and between 0.5 and 1.65 % in silt. Finally, in a wider study, Amoroso et al. (2014) concluded that γ_{DMT} could vary from 0.015 to 0.30 % in sands and from 0.23 to 1.75 % in silts and clays, whereas in soft clays, γ_{DMT} is higher than 2 %. To assess the in situ stiffness decay, Amoroso et al. (2014) suggested the following procedure:

(a) SDMT data obtained at the same depth of each available reference stiffness decay curve are used. A working strain modulus G_{DMT} is derived from M_{DMT} and normalized by its small-strain value, G_0, derived from V_S;
(b) The G_{DMT}/G_0 horizontal ordinate line is superimposed to the same-depth experimental stiffness decay curve in such a way that the data point ordinate matches the reference stiffness decay curve;

FIG. 8 Stiffness obtained from CID TRXs on natural soil specimens consolidated at 50 kPa: (*A*) BH1, depth 1 m; (*B*) BH2, depth 1 m; (*C*) BH 2, depth 3.4 m.

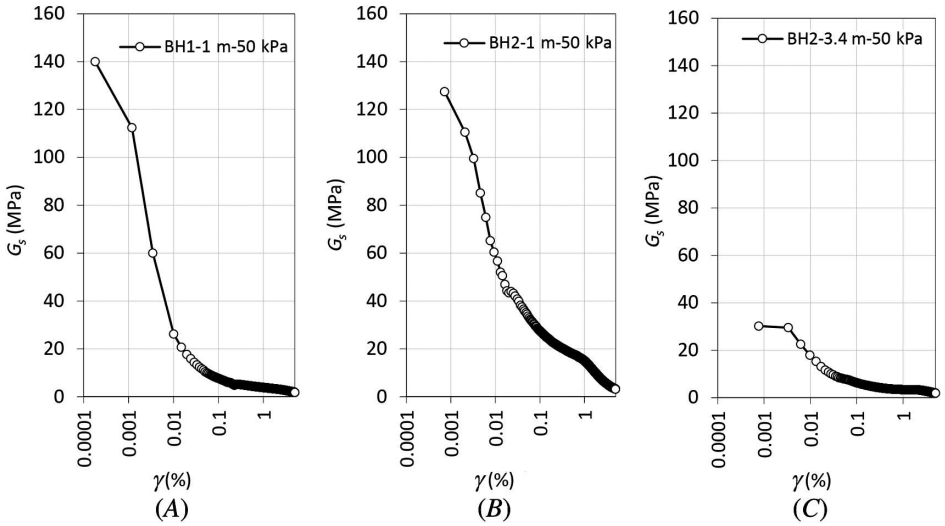

(c) The "intersection" of the G_{DMT}/G_0 horizontal ordinate line with the stiffness decay curve provides a shear strain value, referred to here as γ_{DMT}.

This methodology was applied in this study to test its efficiency in the case of residual soils. Table 7 presents the summary of the obtained results, while figures 9 and 10 represent the SDMT-TRX data related to artificial and natural specimens, respectively. In artificial specimens, triaxial data reveal that the increase in cementation level is followed by an increase in the working strain modulus (G_{DMT}) and decrease in the strain level (γ_{DMT}). In natural specimens, the maximum stiffness obtained at small strain in TRXs converges to the same order of magnitude of the one obtained via shear wave velocities, sustaining the good quality achieved in the sampling processes. Corresponding γ_{DMT} falls within 0.0023 and 0.0089 %, one order of magnitude lower than those proposed by Amoroso et al. (2014) for sedimentary soils with similar grain size (for sands $\gamma_{DMT} \approx 0.015$–$0.30$ %), which probably affects the application of the model in these soils.

Finally, if similar maximum deviatoric stresses are considered in both naturally and artificially cemented specimens, it is possible to observe that behaviors are quite different, with a higher working strain modulus in

TABLE 7
Summary of CID triaxial and SDMT tests in the artificial and natural cemented samples for the same level of confinement stress

Parameter	Rem 0	Mix 1	Mix 2	BH1	BH2	BH2
Type of Sample		Artificial			Natural	
Depth, m	1.04	1.02	1.02	1	1	3.4
SDMT	CCC	CCC	CCC	1	6	6
G_0 MPa (from SDMT)	84.6	102.4	200.0	137.6	108.6	140.4
G_0 MPa (from CID/TRX)	45.9	95.7	214.1	101.1	99.5	101.4
V_s, m/s	230	260	362	256	236	257
M_{DMT}, MPa	10.0	25.3	76.1	243.1	215.8	341.3
G_{DMT}, MPa	2.85	7.22	21.75	69.45	61.65	45.18
γ_{DMT}, %	1.2000	0.3000	0.018	0.00265	0.00890	0.0024
G_{DMT}/G_0	0.034	0.070	0.109	0.50	0.568	0.32

FIG. 9 Laboratory G/G_0-γ curves obtained from CID TRXs consolidated at 50 kPa and superimposed (G/G_0) DMT data points of artificially cemented soils by the DMT test, where G_0 is obtained by V_s seismic measurements (SM): (*A*) Rem 0; (*B*) Mix 1; (*C*) Mix 2.

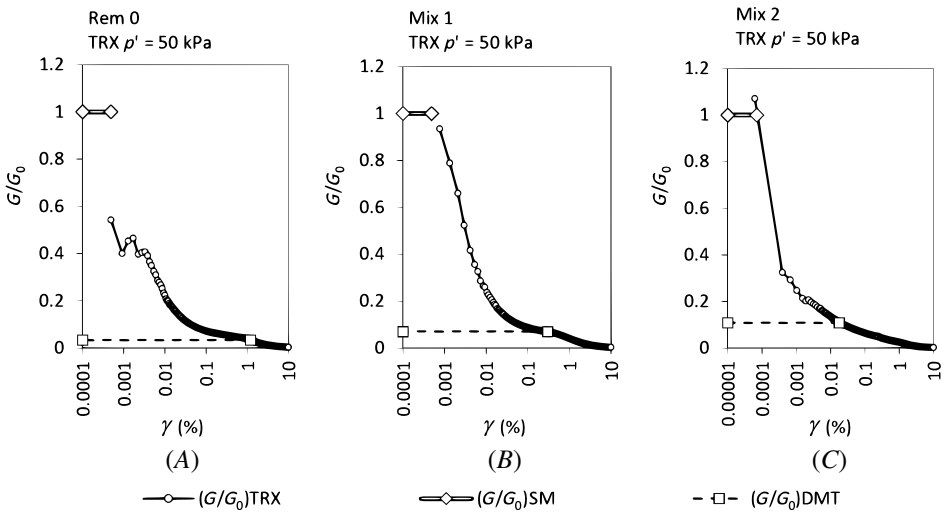

FIG. 10 Laboratory G/G_0-γ curves obtained from CID TRXs consolidated at 50 kPa and superimposed (G/G_0) DMT data points of natural granitic residual soils in Guarda, where G_0 is obtained by V_s seismic measurements in the SDMT test: (*A*) BH1-SDMT1, depth = 1 m; (*B*) BH2-SDMT6, depth = 1.0 m; (*C*) BH2-SDMT6, depth=3.4 m.

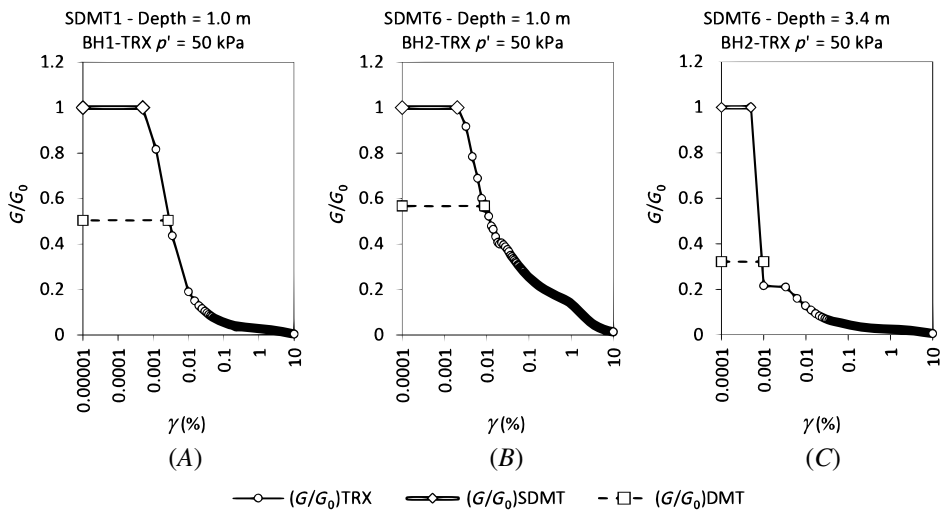

natural samples (fig. 11). This situation is related to the soil fabric, which is quite different in natural samples and artificial mixtures, as can be observed in stress-strain curves (fig. 12) of the specimens consolidated at 50 kPa for natural soil (BH1-TRX-depth = 1.0), artificial mixtures (Mix 1 and 2), and destructured soil (Rem 0). As observed, the peak deviatoric stress in the natural soil is mobilized at higher axial strains when compared with artificial soils, independently of cementation level. The effect of cementation structure is quite evident when comparing the cemented and the noncemented specimens.

FIG. 11

Laboratory G/G_0-γ curves obtained from CID TRXs consolidated at 50 kPa and superimposed (G/G_0) DMT data points of natural and artificially cemented soils; where G_0 is obtained by V_s seismic measurements (SM): (*A*) natural specimen BH1 and SDMT1 depth = 1.0 m; (*B*) artificially cemented specimen CCC in Mix 2.

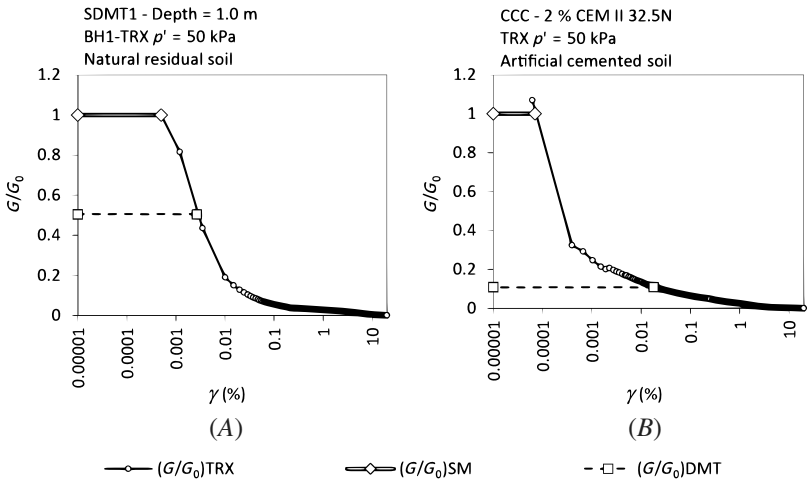

FIG. 12 Stress-strain relationships of CID TRXs performed at 50 kPa of confining pressure in natural specimen BH1 TRX depth = 1.0 m, artificially cemented specimens Mix 1 and Mix 2, and destructured specimen Rem 0: (*A*) Deviatoric stress-axial strain relationship; (*B*) Volumetric strain-axial strain relationship.

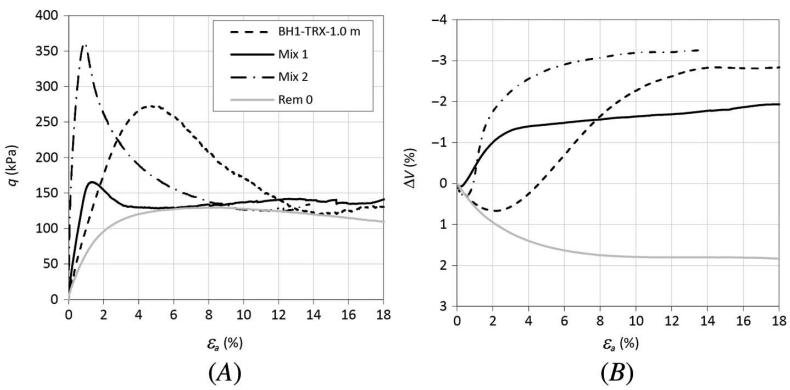

Proposed Numerical *G*-γ Decay Curves

HYPERBOLIC MODEL

Most of the current methods for representing the nonlinear stress-strain behavior of sedimentary soils from small-to-medium strain levels are based on a hyperbolic stress-strain relationship, which may be expressed by the following equations:

$$\frac{G}{G_0} = \frac{1}{1 + \left(\frac{\gamma}{\gamma_r}\right)} \tag{3}$$

$$\gamma_r = \frac{\tau_{max}}{G_0} \tag{4}$$

where:

G_0 = maximum shear modulus,
G = shear modulus,

τ = shear strength,
τ_{max} = maximum shear strength,
γ = shear strain, and
γ_r = reference shear strain.
Combining the equations (3) and (4), the following equation is obtained:

$$\frac{G}{G_0} = 1 - \frac{\tau}{\tau_{max}} \tag{5}$$

The rate of reduction of the secant shear modulus G with the increase of the shear strain γ is plotted conventionally as G (or G/G_0) versus γ on a logarithmic axis. Several authors (Hardin and Drnevich 1972; Bellotti et al. 1989; Byrne, Salgado, and Howie n.d.; Fahey and Carter 1993; Fahey 1998; Rodrigues et al. n.d.) have proposed the hyperbolic model to represent the nonlinear stress-strain behavior in PMTs, mostly for sedimentary soils. Following this approach, Amoroso et al. (2014) suggested equation (6) to represent the hyperbolic stress-strain behavior by means of using SDMT data in sedimentary soils, namely through the maximum shear modulus and the shear modulus for a reference strain:

$$\frac{G}{G_0} = \frac{1}{1 + \left(\frac{G_0}{G_{DMT}} - 1\right)\frac{\gamma}{\gamma_{DMT}}} \tag{6}$$

According to this representation, the experimental CCC data and the corresponding TRXs were used to support the construction of the hyperbolic equation and study the efficiency of the model previewing the behavior of residual soils. The ratio G_{DMT}/G_0 obtained from SDMT and the estimated shear strain γ_{DMT} were used to plot the corresponding hyperbolic curves of the tests. The results of natural soils are shown in **figure 13** plotted together with the curves obtained from SDMT using equation (6) and the coupled values of G_{DMT}/G_0 versus γ_{DMT} as well as the simulation of the behavior by the hyperbolic model. The figure shows that, when applied to granitic residual soils, the hyperbolic approach proposed by Amoroso et al. (2014) generates a reasonable agreement to the real behavior at a small-strain level, while at medium and high strain levels there is an underestimation of the stiffness of the natural soil.

FIG. 13 Hyperbolic model and laboratory G/G_0-γ curves superimposed from the (G/G_0) DMT data points of natural granitic residual soils of Guarda; where G_0 is obtained by V_s seismic measurements (SM) in the SDMT test: (*A*) BH1-TRX, depth = 1 m; (*B*) BH2-TRX, depth = 1.0 m; (*C*) BH2-TRX, depth = 3.4 m.

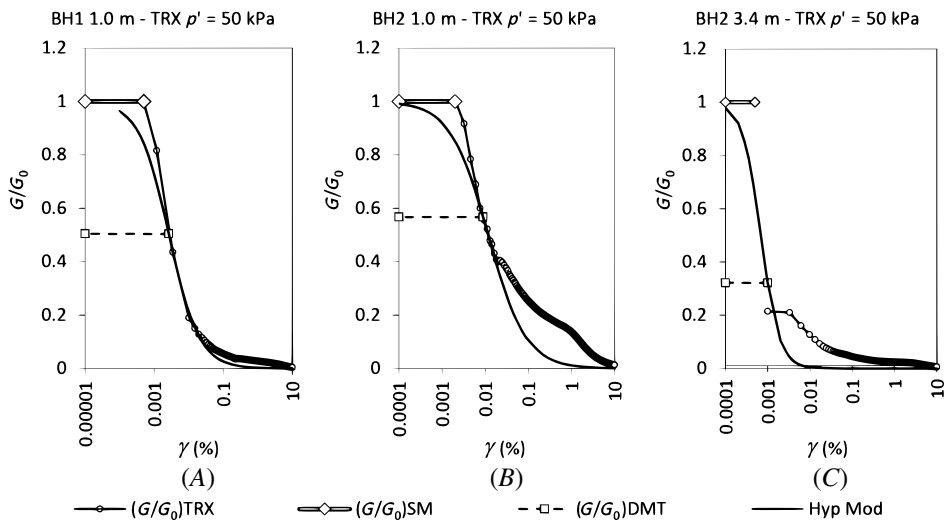

On its turn, figure 14 shows that the hyperbolic model fits the TRX curve well for Rem 0 for $\gamma > 1$ %, i.e., at high strain levels. For medium strain levels, the agreement seems poor.

On the other hand, for the same strain levels in cemented mixtures, the model generates a poorly fitted decay curve and quite different results, getting worse with increasing cementation level. In this case, the artificial experimental frame represents the DMT-derived hyperbolic curve measured exactly in the same conditions of cementation level and void ratios of the triaxial reference curve. The most probable reason for these deviations should be related to the value of γ_{DMT} because it varies not only with G_{DMT}/G_0 but also with the cementation level. Intermediate mathematical analysis indicate the probability of this explanation.

LOGISTIC MODEL

The deviations generated by the hyperbolic model proposed by Amoroso et al. (2014) when representing (artificial and natural) cemented specimen results, suggested the introduction in the formulation of "cementation parameters," relying only on SDMT data. The approach was to follow a more generalized expression than the one proposed by Amoroso's hyperbolic model, represented by the logistic curve expressed in equation (7):

$$G(\gamma) = \frac{a}{\left(1 + e^{-b(\log(\gamma) - c)}\right)}, \gamma > 0 \tag{7}$$

where:

$a = \lim_{\gamma \to 0} G(\gamma)$ represents the logistic curve horizontal asymptote,

$b < 0$ represents the gradient of the curve, and

c represents the natural logarithm transformed x-value of the curve's midpoint.

Note that in taking $a = G_0$, $b = -1$, and $c = -\log(\frac{G_0 - G_{DMT}}{G_{DMT} \times \gamma_{DMT}})$, equation (6) will be obtained.

The logistic model was built finding the best curve type that "explains" triaxial data and, departing from there, finding a correlation between the (a, b, c) triplet and SDMT parameters. All the stiffness values with strains lower than the peak resistance obtained from the TRX were considered in the analysis, while DMT test parameters were used to fit the logistic curve to the multiple points (γ, G/G_0) acquired via TRX.

FIG. 14 Hyperbolic model and laboratory G/G_0-γ curves superimposed on the (G/G_0) DMT data points of artificially cemented granitic residual soils of Guarda, where G_0 is obtained by V_s seismic measurements (SM): (*A*) Rem 0; (*B*) Mix 1; (*C*) Mix 2.

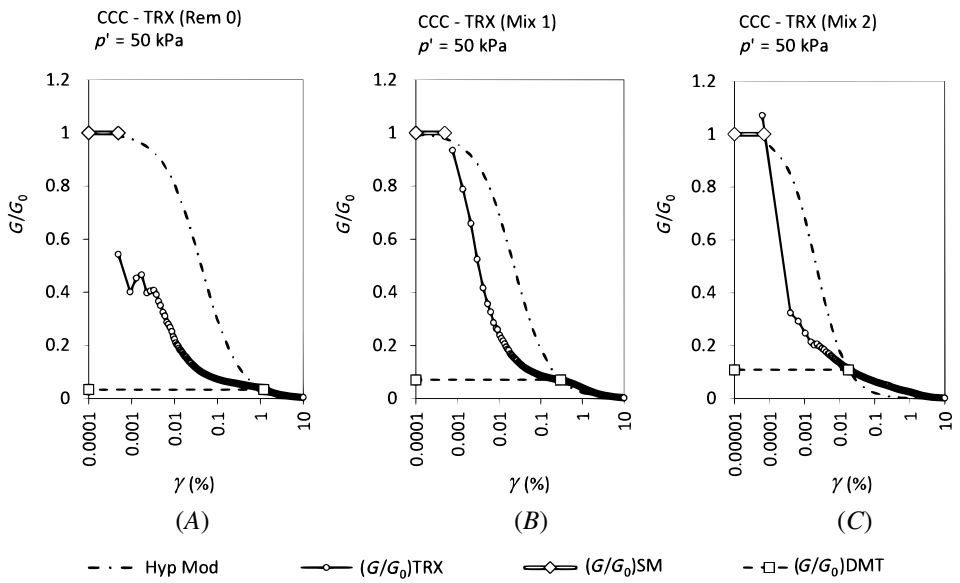

Considering the model based only on SDMT data, the parameter a should be equal to G_0 since $b < 0$ and $\lim_{\gamma \to 0} \frac{G}{G_0} = 1$. On its turn, the cementation influence should be related to the remaining b and c parameters using DMT parameters known as sensitive to cementation (like K_D and the virtual overconsolidation ratio, $vOCR$, as defined by Cruz in 2010), stiffness (like E_D, M_{DMT}, and G_0), or both. Accordingly, the small-strain shear modulus (G_0), constrained modulus (M_{DMT}), working strain shear modulus (G_{DMT}), virtual overconsolidation ratio ($vOCR$) and correspondent virtual preconsolidation effective stress ($v\sigma'_{vc}$), current effective vertical stress (σ'_{v0}), ratio G_0/G_{DMT}, dilatometer modulus (E_D), and horizontal stress index (K_D) were tested to provide the most relevant fit. For each data set resulting from the experiences described in the previous sections, the logistical model was adjusted regarding its parameters, ($a = G_0$), b, and c, using weighted least squares since the data sets were not uniformly distributed along all the gamma values. Thereafter, each (a, b, c) triplet that provided the best fit to the respective data set was combined with all the SDMT parameters and several combinations/functions of those parameters were tested using MATLAB R2016b. The best fits show the parameter b correlated with $vOCR$ (cementation) and the parameter c correlated with a combination of G_0 (in MPa) and K_D (maximum stiffness and cementation) represented in equations (8) and (9). The virtual overconsolidation ratio, $vOCR$, is calculated by the equation proposed by Marchetti and Crapps (1981) for sedimentary soils. The term virtual is applied because the concept of overconsolidation ratio is not applicable to residual soils (Cruz 2010).

$$b = 0.0004406 vOCR - 0.5591, \text{ with } r = -0.55 \tag{8}$$

$$c = -4.041 - 0.02774 G_0 + 0.03388 K_D \text{ with } r = 0.93 \tag{9}$$

Replacing these in the original formulation (equation (7)), equation (10) will be obtained:

$$G = \frac{G_0}{\left(1 + e^{-(-0.0004406 * vOCR - 0.5591)(\log(\gamma) - (-4.041 - 0.02774 * G_0 + 0.03388 * K_D))}\right)} \tag{10}$$

The results obtained applying this model in the natural and artificial residual soils are respectively shown in figures 15 and 16, both comparing the logistic curves with Amoroso et al. (2014)'s hyperbolic model and the TRX

FIG. 15 Comparison between the hyperbolic model, logistic model, and laboratory TRX G/G_0-γ of the natural granitic residual soils of Guarda; where G_0 is obtained by V_s seismic measurements (SM) in the SDMT test: (*A*) BH1-TRX, depth = 1 m; (*B*) BH2-TRX, depth = 1.0 m; (*C*) BH2-TRX, depth = 3.4 m.

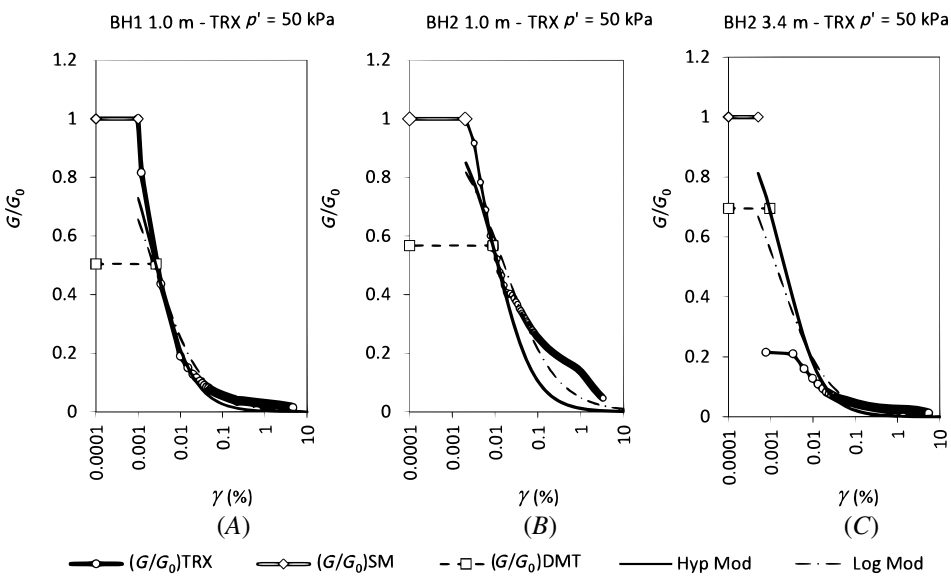

FIG. 16 Logistic model, hyperbolic model, and laboratory triaxial values of G/G_O-γ curves (TRX) superimposed on the (G/G_O) DMT data points of artificially cemented granitic residual soils of Guarda; where G_O is obtained by V_s seismic measurements (SM): (*A*) Rem 0; (*B*) Mix 1; (*C*) Mix 2.

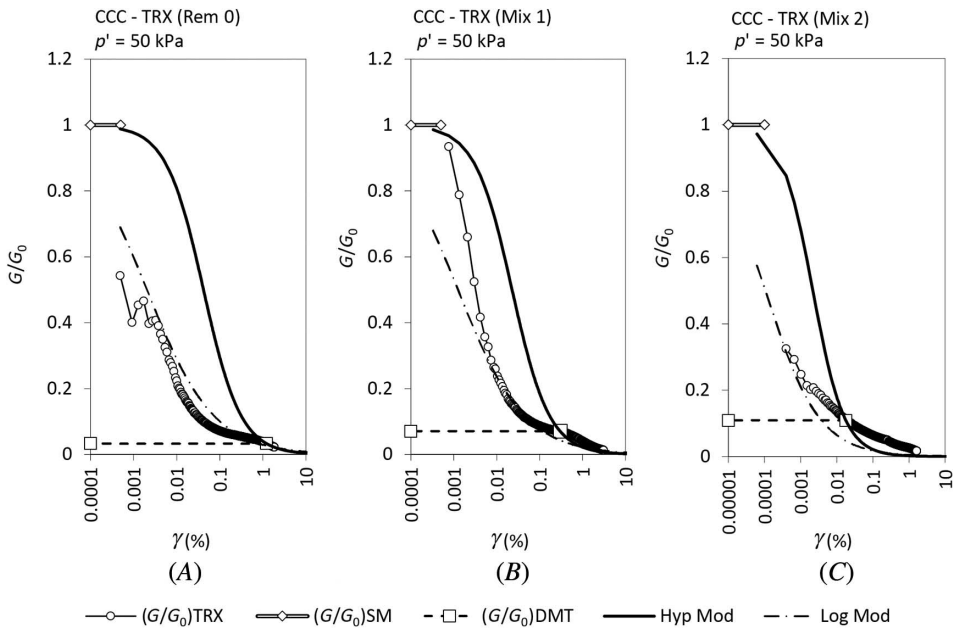

TABLE 8
Absolute mean error and average absolute percent error of G/G_O

Test	γ_{max}, %	Absolute Mean Error		Average Absolute Percent Error	
		Hyperbolic Model	Logistic Model	Hyperbolic Model	Logistic Model
DMT1-1.0-50	4.658	0.0202	0.0142	89.8	65.5
DMT6-1.0-50	1.892	0.1255	0.0755	82.1	51.6
DMT6-3.4-50	5.640	0.0209	0.0154	90.3	67.0
Rem 0	1.503	0.0849	0.0135	94.6	20.0
Mix 1	1.658	0.0651	0.0227	60.8	30.0
Mix 2	1.435	0.0330	0.0317	81.7	77.2

results. These figures clearly show the better adherence of the logistic (generalized) model to the TRX data when compared with the model proposed by Amoroso et al. (2014). The statistical determinations of absolute mean error and average absolute percent error between the ratio G/G_0 generated by the two models and the triaxial reference data clearly supports this conclusion (Table 8).

Conclusions

Based on experimental framework and mathematical analysis, a logistic model was proposed to predict in situ stiffness decay curves with strain level (G-γ curves or similar) in granitic residual soils of Guarda from SDMT test data. The usefulness of SDMT for that purpose is sustained by the possibility of having independent measurements at small (G_0) and working strain (I_D, E_D, K_D) levels; the partially preserved cementation of the soil involved

in the measurement after test penetration and its sensitivity to cementation variations is referred to in several publications based in these Portuguese granitic environments (see Cruz 2010).

The cementation structure of natural soils influences the stiffness behavior, as revealed by the TRX results presented in the article. The research showed that the hyperbolic model based on SDMT data proposed by Amoroso et al. (2014) only reveals good convergence to the triaxial experimental curves of a destructured, noncemented specimen. In naturally and artificially cemented soils, the model did not show the same efficiency. Mathematical analysis proved that this variation was probably related to the influence of the cementation level. The deviation is more pronounced with the cementation increase.

The logistic model proposed herein was built finding the best curve type that "explains" the whole set of triaxial data with this experiment. Once the logistic curve (best fit) was settled, SDMT data were used to calibrate the parameters (a, b, c) that place the curve over the observed triaxial γ decay obtained for cemented (artificially or naturally) and noncemented specimens. The best fits show parameter a represented by G_0, parameter b correlated with $vOCR$ (cementation), and parameter c correlated with a combination of G_0 and K_D (maximum stiffness and cementation). The proposed model was constructed based on a limited set of experimental laboratorial data of natural and artificially cemented granitic soils from Guarda. It is possible that some deviations occur when applied to other contexts, especially in the case of residual soils from other lithological types or with origins in other environments. It is expected that the model will fit in the case of granitic soils from other Portuguese massifs since the mechanical behavior is typically convergent.

References

Almeida, F., L. Café, N. Cruz, and C. Rodrigues. n.d. "Laboratorial S-Wave Measurements with Buried Geophones in a Large Calibration Box." Paper presented at the Fourth International Conference on Geotechnical and Geophysical Site Characterization, Porto de Galinhas, Brazil, September 18–21, 2012.

Alvarado, G., M. R. Coop, and S. Willson. 2012. "On the Role of Bond Breakage due to Unloading in the Behaviour of Weak Sandstones." *Géotechnique* 62, no. 4 (April): 303–316. https://doi.org/10.1680/geot.8.P.017

Amoroso, S., P. Monaco, B. M. Lehane, and D. Marchetti. 2014. "Examination of the Potential of the Seismic Dilatometer (SDMT) to Estimate In Situ Stiffness Decay Curves in Various Soil Types." *Soils and Rocks* 37, no. 3 (September–December): 177–194.

ASTM International. 2015. *Standard Test Method for Performing the Flat Plate Dilatometer*. ASTM D6635–15. West Conshohocken, PA: ASTM International, approved November 1, 2015. https://doi.org/10.1520/D6635-15

ASTM International. 2019. *Standard Test Methods for Downhole Seismic Testing*. ASTM D7400/D7400M-19. West Conshohocken, PA: ASTM International, approved February 1, 2019. https://doi.org/10.1520/D7400_D7400M-19

Baligh, M. M. and R. F. Scott. 1975. "Quasi-Static Deep Penetration in Clays." *Journal of the Geotechnical Engineering Division* 101, no. 11: 1119–1133.

Bellotti, R., V. Ghionna, M. Jamiolkowski, P. K. Robertson, and R. W. Peterson. 1989. "Interpretation of Moduli from Self-Boring Pressuremeter Tests in Sand." *Géotechnique* 39, no. 2 (June): 269–292. https://doi.org/10.1680/geot.1989.39.2.269

Byrne, P. M., F. M. Salgado, and J. A. Howie. n.d. "Relationship between the Unload Shear Modulus from Pressuremeter Tests and the Maximum Shear Modulus for Sand." Paper presented at the Third International Symposium on Pressuremeters, Oxford, UK, April 2–6, 1990.

Clayton, C. R. I. and G. Heymann. 2001. "The Stiffness of Geomaterials at Very Small Strains." *Géotechnique* 51, no. 3 (April): 245–255. https://doi.org/10.1680/geot.2001.51.3.245

COBA. 2003. *Carta Geotécnica do Porto*. Porto, Portugal: Porto City Hall.

Coop, M. R. and S. M. Willson. 2003. "Behavior of Hydrocarbon Reservoir Sands and Sandstones." *Journal of Geotechnical and Geoenvironmental Engineering* 129, no. 11 (November): 1010–1019. https://doi.org/10.1061/(ASCE)1090-0241(2003)129:11(1010)

Cruz, N. B. F. "Modelling Geomechanics of Residual Soils by DMT Tests." PhD thesis, University of Porto, 2010.

Cuccovillo, T. and M. R. Coop. 1997. "Yielding and Pre-failure Deformation of Structured Sands." *Géotechnique* 47, no. 3 (June): 491–508. https://doi.org/10.1680/geot.1997.47.3.491

Di Mariano, A., S. Amoroso, M. Arroyo, P. Monaco, and A. Gens. 2019. "SDMT-Based Numerical Analyses of Deep Excavation in Soft Soil." *Journal of Geotechnical and Geoenvironmental Engineering* 145, no. 1 (January): 04018102. https://doi.org/10.1061/(ASCE)GT.1943-5606.0001993

Fahey, M. 1998. "Deformation and In Situ Stress Measurement." In *Geotechnical Site Characterization*. Rotterdam, the Netherlands: A. A. Balkema.

Fahey, M. and J. P. Carter. 1993. "A Finite Element Study of the Pressuremeter Test in Sand Using a Nonlinear Elastic Plastic Model." *Canadian Geotechnical Journal* 30, no. 2 (April): 348–362. https://doi.org/10.1139/t93-029

Finno, R. J. 1993. "Analytical Interpretation of Dilatometer Penetration through Saturated Cohesive Soils." *Géotechnique* 43, no. 2 (June): 241–254. https://doi.org/10.1680/geot.1993.43.2.241

Hardin, B. O. and V. P. Drnevich. 1972. "Shear Modulus and Damping in Soils: Design Equations and Curves." *Journal of Soil Mechanics and Foundation Division* 98, no. sm7 (July): 667–692.

Huang, A.-B. 1989. "Strain-Path Analyses for Arbitrary Three-Dimensional Penetrometers." *International Journal for Numerical and Analytical Methods in Geomechanics* 13, no. 5 (September/October): 551–564. https://doi.org/10.1002/nag.1610130507

Ishihara, K. n.d. "Estimate of Relative Density from In-Situ Penetration Tests." Paper presented at the International Conference on In Situ Measurement of Soil Properties and Case Histories, Bali, Indonesia, May 21–24, 2001.

Lumb, P. 1962. "The Properties of Decomposed Granite." *Géotechnique* 12, no. 3 (September): 226–243. https://doi.org/10.1680/geot.1962.12.3.226

Malandraki, V. and D. G. Toll. 1996. "The Definition of Yield for Bonded Materials." *Geotechnical & Geological Engineering* 14, no. 1 (March): 67–82. https://doi.org/10.1007/BF00431235

Malandraki, V. and D. G. Toll. 2001. "Triaxial Tests on a Weakly Bonded Soil with Changes in Stress Path." *Journal of Geotechnical and Geoenvironmental Engineering* 127, no. 3 (March): 282–291. https://doi.org/10.1061/(ASCE)1090-0241(2001)127:3(282)

Marchetti, S. and D. K. Crapps. 1981. *Flat Dilatometer Manual*. Gainesville, FL: GPE, Inc.

Marchetti, S. 1980. "In Situ Tests by Flat Dilatometer." *Journal of Geotechnical Engineering Division* 106, no. 3 (March): 299–321.

Marchetti, S., P. Monaco, G. Totani, and D. Marchetti. 2008. "In Situ Tests by Seismic Dilatometer (SDMT)." In *From Research to Practice in Geotechnical Engineering*, 292–311. Reston, VA: American Society of Civil Engineers.

Mayne, P. W. n.d. "Stress-Strain-Strength-Flow Parameters from Enhanced In-Situ Tests." Paper presented at the International Conference In-Situ Measurement of Soil Properties and Case Histories, Bali, Indonesia, May 21–24, 2001.

Monaco, P., S. Amoroso, S. Marchetti, D. Marchetti, G. Totani, S. Cola, and P. Simonini. 2014. "Overconsolidation and Stiffness of Venice Lagoon Sands and Silts from SDMT and CPTU." *Journal of Geotechnical and Geoenvironmental Engineering* 140, no. 1 (January): 215–227. https://doi.org/10.1061/(ASCE)GT.1943-5606.0000965

Monaco, P., S. Marchetti, G. Totani, and D. Marchetti. n.d. "Interrelationship between Small Strain Modulus G_0 and Operative Modulus." Paper presented at the International Conference on Performance-Based Design in Earthquake Geotechnical Engineering, Tokyo, Japan, June 15–18, 2009.

Monaco, P., G. Totani, and M. Calabrese. n.d. "DMT-Predicted vs Observed Settlements: A Review of the Available Experience." Paper presented at the Second International Conference on the Flat Dilatometer, Washington, DC, April 2–5, 2006.

Rocchi, I. and M. R. Coop. 2015. "The Effects of Weathering on the Physical and Mechanical Properties of a Granitic Saprolite." *Géotechnique* 65, no. 6 (June): 482–493. https://doi.org/10.1680/geot.14.P.177

Rodrigues, C., S. Amoroso, N. Cruz, and J. Cruz. n.d. "G-γ Decay Curves in Granitic Residual Soils by Seismic Dilatometer." Paper presented at the Fifth International Conference on Geotechnical and Geophysical Site Characterization (ISC'5), Gold Coast, Australia, September 5–9, 2016.

Rodrigues, C. M. G. "Caracterização geotécnica e estudo do comportamento geomecânico de um saprólito granítico da Guarda [Geotechnical Characterization and Geomechanical Behaviour Analysis of a Granite Saprolite from Guarda Granites]." PhD Thesis, University of Coimbra, 2003.

Viana da Fonseca, A. and R. Q. Coutinho. n.d. "Characterization of Residual Soils." Paper presented at the Third International Conference on Site Characterization (ISC'3), Taipei, Taiwan, April 1–4, 2008.

Whittle, A. J. and C. P. Aubeny. n.d. "The Effects of Installation Disturbance on Interpretation of In Situ Tests in Clay." Paper presented at the Wroth Memorial Symposium, Oxford, UK, July 27–29, 1992.